www.czasopisma.pan.pl PAN www.journals.pan.pl
POLSKA AKADEMIA NAUK
Opto-Electronics Review 25 (2017) 251–262

Contents lists available at ScienceDirect

Opto-Electronics Review

journal homepage: http://www.journals.elsevier.com/opto-electronics review

Characterization of GaN nanostructures by electron field and photo-field emission

V. Litovchenko, A. Evtukh*, A. Grygoriev

V. Lashkaryov Institute of Semiconductor Physics, 41 Nauki ave., 03028 Kyiv, Ukraine

ARTICLE INFO

Article history:
Received 11 August 2016
Accepted 16 December 2016
Available online 17 August 2017

Keywords:
GaN nanostructures
Electron field emission
Photo-field emission
Electron redistribution
Illumination
Quantum effects

ABSTRACT

The electron field and photo-field emission from GaN nanostructures has been analyzed in this review. In order to explain the obtained experimental results, a model was proposed taking into account the change in carrier concentration distribution in the main and the satellite valley during the emission process. The lowering of work function (due to the increased number of carriers in the satellite valley) can explain the decrease in the Fowler-Nordheim plot slope. It was shown that the energy difference between the main and satellite valley in GaN was decreased in the case of quantum confinement, thus increasing the probability of electron transition from Γ to X valley at same electric fields.

Investigations of electron photo-field emission demonstrated that the Fowler–Nordheim plots of the emission current have different slopes for nonilluminated and illuminated devices. A model based on the electron emission from valleys having different specific electron affinities is proposed to explain the experimental results. In the absence of illumination the emission takes place only from the lower valley. Upon UV illumination and presence of a high electric field at the emitter tip, the upper valley of the conduction band appears to be occupied by electrons generated at the valence band.

© 2017 Association of Polish Electrical Engineers (SEP). Published by Elsevier B.V. All rights reserved.

1. Introduction

Wide bandgap semiconductors, such as GaN, are very promising for novel applications in optoelectronics, solid-state and vacuum nanoelectronic devices. Tremendous progress both in the science and engineering of group-III nitrides and devices based on them has been made [1].

The large bandgap of group-III nitrides and the chemical and thermal stability allow new applications. Important are also the positive characteristics such as high saturation drift velocity of electrons of nearly 3×10^7 cm/s [2] and extremely high breakdown field strengths of $(3–5) \times 10^6$ V/cm [3]. Furthermore, these materials find application for various sensor concepts because of their large piezoelectric coefficients and robustness in harsh environments [4–7].

One of the most amazing properties of III-nitride semiconductors, particularly the family of direct-bandgap semiconductors, is light emission in response to excitation mainly by means of electrical injection of minority carriers or optical and electrical beam excitation, the discovery of which revolutionized the field of optoelectronics. Specifically, light emission induced by electrical injection of minority carriers, which is termed electroluminescence (EL), has seen the most practical applications. The direct bandgap nitride semiconductors, ranging from about 0.8–6.2 eV, are ideally suited for a large variety of detectors, especially in the ultraviolet (UV) range as there are currently no serious semiconductor-based competing technologies. A large absorption coefficient (a result of the direct bandgap) and the ability to detect the UV- and solar-blind regions of the spectrum make them very attractive detector candidates.

New vacuum nanoelectronic devices can help to overcome the frequency and power limitations of solid state devices [8,9]. Field emission based vacuum micro-nano-devices (e.g. miniaturized tubes) are promising for amplification and generation of high frequency electromagnetic waves [8,10,11]. In such devices, electron transport is performed through vacuum without scattering, as is in case of solid state components, therefore setting up the basis for attaining ultrahigh frequency operation. Efficient electron field emission cathodes are here of major importance. New developments in field emitter arrays (FEAs) are therefore discussed and experimentally investigated. FEAs with high current densities are considered as promising sources of cold electrons in miniature tubes for millimeter-wave generation.

Functional field emitter based on nitride materials shows new effects, which can be used for miniaturized vacuum devices, as well

* Corresponding author.
E-mail address: anatoliy.evtukh@gmail.com (A. Evtukh).

http://dx.doi.org/10.1016/j.opelre.2017.06.004
1230-3402/© 2017 Association of Polish Electrical Engineers (SEP). Published by Elsevier B.V. All rights reserved.

as new sensors. They open the possibility for density modulation of the electron beam with a gate electrode or photo-modulation instead of velocity modulation after electron emission in the vacuum tube. The advantages obtained by pre-bunching the beam are high efficiency and significant reduction in the required RF interaction length in the tube, thereby simplifying beam transport magnetics and reducing the weight. Devices with high-power and high- efficiency can be obtained [12,13].

Currently one-dimensional and three-dimensional nanoscale materials are under focus due to their unique electronic, optical and magnetic properties, as well as potential applications in constructing novel nanodevices [14,15].

Gallium nitride (GaN), as a wide-bandgap semiconductor, has attracted a lot of attention as a material for electron field emission (EFE) devices [16]. It has strong chemical and mechanical stability, high melting point (2600 K), and low electron affinity of 2.7–3.3 eV [17–21]. Moreover, FE cathodes based on GaN have longer lifetimes than based on Si or other conventional semiconductors.

There are many researches on FE from GaN films [18,22] and pyramid arrays [23]. It was reported that the pyramid or rough-surface GaN increased the field enhancement factor (β), lowering the applied voltage for the electron emission. Thus, further enhancement of EFE characteristics is expected by the one-dimensional (1D) GaN structures. Various GaN nanowires and nanorods were fabricated and their field emission properties were investigated [24–28]. In recent years many attempts have been made to synthesize one-dimensional and three-dimensional GaN morphologies. Up to now, one-dimensional and quasi-one-dimensional GaN nanorods [15], nanowires [29], nanotubes [30], nanoribbons [31], nanobelts [32] and prismatic rods and cone nanowires [27] have been synthesized. There are also some reports about three-dimensional GaN nanostructures [33–35].

Such different GaN morphologies were produced by numerous methods such as sol–gel method, simple thermal evaporation method [24,36], templates method, pulse laser ablation (PLA) [25,37,38], and chemical vapour deposition (CVD) method [36,37,28–40]. The 1D GaN structures were obtained either by NW growth or GaN etching, where etching is widely used for GaN surface roughening and nanotip formation [18,41,42].

Photoelectric field emission has attracted great interest from two points of view: drastic improvement of beam brightness due to increased emission current [43] and generation of modulated electron beams by means of photomixing. The ability to generate a high frequency modulated beam directly at the cathode, known as prebunching, through pulsed optical excitation would benefit vacuum nanoelectronics devices. A photo-assisted field emission spectroscopy method has been developed for characterization of the energy bands of wide bandgap materials used in optoelectronics, solid-state and vacuum nanoelectronic devices.

2. Intervalley carrier redistribution in nanostructured semiconductors at electron field emission

The intervalley redistribution of hot electron in semiconductor materials plays the principal role in a set of important physical effects such as Gunn oscillation effect, HEMT (High Electron Mobility Transistor) transistors, electron field emission, etc. [44–49].

However, for some perspective materials, in particular GaN, the external electric field is not enough for intervalley redistribution by conventional ways, when the bulk structures of the experimental samples is used [47], due to the scattering on rather large energy optical phonon (for GaN $E_{ph} \approx 90$ meV), large value of the electron-phonon interaction factor and, as a result, very low optical phonon lifetime $\tau_{sp} \approx 3 \times 10^{-14}$ s, whereas experimental times of the spontaneous decay gives substantially larger values $\tau_{dec} \approx 8.5 \times 10^{-14}$. That means, that even at ultra short electric pulse ($\tau_t \leq 10$ ps) [47,48], the applied electric field pulses, usually used in experiments, is less on the order the values of the presented τ_{vo}, measured with help of the optical time decay τ method or obtained by Monte Carlo theoretical calculation [46–52].

Hence, the problem appears how to obtain in GaN (and similar wide bandgap semiconductors) high energy hot electrons, with energy enough for intervalley redistribution. The mechanism of the "phonon throat" for quantum well phonons has been proposed in [44,45] for solution of this problem in relation to HEMT. The barrier for scattering of electron energy appears due to the quantization of the phonon spectra in narrow potential wells and, as a result, substantial decreasing of the electron-phonon interaction. This allows in such a way to obtain the rather high value of carriers mobility in quantum channel, and hence, high frequency HEMT transistors.

Electron field emission offers a new possibility for the study of band structure parameters, such as intervalley energy difference, electron affinity from different conduction band valleys, and intervalley free electron redistribution due to heating of carriers by external high electrical fields. The conelike shape and small size of the field emitter cathodes allow reduction in lattice overheating, which is a serious problem for devices operating at high electric fields [53–61]. Important peculiarities of the wide bandgap semiconductors are their large intervalley distance (1–2 eV or higher), as well as charge trapping and piezoelectric phenomena [55,62,63]. The conduction band nonparabolicity can also play a significant role leading to the decrease in the electron mobility. Under such circumstances, the drift mobility at high electrical fields decreases even without any carrier redistribution taking place from the central to the upper (satellite) valley [57]. At extremely high electrical fields, additional field emission mechanisms can appear, namely, the emission from charged traps in the wide forbidden gap, localized on the surface or in the bulk, and emission from the valence band. In the case of wide bandgap semiconductors, these effects can be substantially suppressed.

Several EFE measurements and simulations for quantum sized cathodes have shown possible transformation of the energy bands [54–60]. The quantum-size effect decreases considerably the intervalley energy difference for cathodes with tip radii of few nanometers [60]. The first theory of field emission from semiconductors was reported in Refs. [64,65]. It was based on degenerated carrier statistics and took into account different electron masses in semiconductor and vacuum.

Additional important features, such as complex many valley structure of the Brillouin zone, hot carrier generation, and intervalley carrier redistribution have been considered in Ref. [52]. Furthermore, the quantum mechanical tunneling process from the backside metal-semiconductor junction is an important mechanism for current transport through thin barriers. The top of the triangular barrier used in the proposed model [52] of the semiconductor-vacuum interface was additionally lowered by the image force potential.

Tunneling probability of electrons from a semiconductor into vacuum has been derived from the time independent Schrödinger equation:

$$-\frac{\hbar^2}{2m_e} \cdot \frac{d^2\Psi}{dx^2} + V(x)\Psi = E\Psi, \tag{1}$$

which can be rewritten as:

$$\frac{d^2\Psi}{dx^2} = \frac{2m_e(V-E)}{\hbar^2}\Psi, \tag{2}$$

where ħ is the normalized Planck constant, Ψ is the wave function, m_e is the effective electron mass, $V(x)$ is the potential relief on the electron path, E is the energy of electron, and x is the tunneling direction from the surface into vacuum (see inset in Fig. 1).

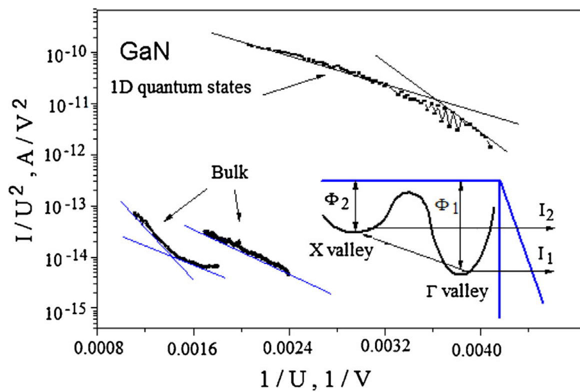

Fig. 1. Experimental I–V characteristics of the field emission current from GaN in F-N coordinates. In the case of bulk material, the difference in two curves is caused by different micrometer radii of curvature for the emitter. The inset shows the schematic energy band diagram of a two-valley semiconductor [52].

Assuming that $V(x) - E$ is independent of position in a section between x and $x + dx$ (Wentzel–Kramers–Brillouin (WKB) approximation), this equation can be solved yielding:

$$\Psi(x + dx) = \Psi(x) \cdot e^{-kdx}, \quad (3)$$

with $k = \frac{\sqrt{2m_e[V(x)-E]}}{\hbar}$.

The minus sign is chosen since it is assumed that the particles move from the left to the right. For a slowly varying potential, the amplitude of the wave function at $x = L$ can be related to the wave function at $x = 0$ through the following equation [66]:

$$\Psi(L) = \Psi(0) \exp\left\{-\int_0^L \frac{\sqrt{2m_e[V(x)-E]}}{\hbar} dx\right\}, \quad (4)$$

where L is the classical turning point (L is the external barrier border that is the last point where an electron is inside of the barrier potential). Eq. (4) is also referred to WKB approximation.

In general, a triangular barrier is assumed to approximate the semiconductor-vacuum interface. The tunneling probability (Θ) can be calculated in the case of the triangular barrier approximation by the following equation [61]:

$$\Theta = \frac{\Psi(L)\Psi^*(L)}{\Psi(0)\Psi^*(0)} = \exp\left\{-\int_0^L \frac{\sqrt{2m_e}}{\hbar}\sqrt{q\chi_0\left(1 - \frac{x}{L}\right)} \mathrm{d}x\right\}, \quad (5)$$

where χ_0 is the barrier height at the cathode-vacuum interface.

The parameter Θ can be evaluated as a function of the electric field F:

$$\Theta_\Delta(F, E) = C \cdot \exp\left(-\frac{4}{3\hbar F} \cdot \sqrt{2m_e(\chi_0 - E)^3}\right), \quad (6)$$

where Θ_Δ is the tunneling probability trough the triangular barrier and C is a constant.

The tunneling current $J_i(F)$ from valley i can be obtained from the product of the density of available electrons n, tunneling probability, and effective drift velocity $v_D{}^*$. The latter can be different from the ordinary determined bulk drift velocity due to the influence of scattering in the barrier. It has been assumed, however, that the barrier does not considerably disturb the field dependence, which is in any case a much weaker function compared with the other multiplier. The velocity corresponds to the average velocity of the carriers approaching the barrier, while the carrier density equals to the density of available electrons (before the barrier) multiplied with the tunneling probability. Based on the above, $J(F)$ can be expressed as:

$$J_{C1}(F) = A_{C1} \int_{E_{C1}}^{E_{C2}} n_1(F, E) \cdot \Theta_1(F, E) \cdot v_{D1}(F, E) dE$$
$$J_{C2}(F) = A_{C2} \int_{E_{C2}}^{\infty} n_2(F, E) \cdot \Theta_2(F, E) \cdot v_{D2}(F, E) dE \quad (7)$$

where $J_{C1}(F)$ is the current from the main valley; $J_{C2}(F)$ is the current from the satellite valley; E_{C1} is the energy position of the main valley, and E_{C2} is the energy position of the satellite valley.

The tunneling current shows consequently an exponential dependence on the 3/2 power of the barrier height, when all other multipliers ($n_1, n_2, v_{D1}, v_{D2}, A_{C1}, A_{C2}$) are constant or differ slightly.

In the well-established F-N approximation, $J_{FN}(F)$ shows only an exponential dependence on the 3/2 power of the barrier height (ϕ) at the cathode-vacuum interface:

$$J_{FN}(F) = C_{FN} \times \frac{F^2}{\phi} \exp(-B\phi^{3/2}/F), \quad (8)$$

where the multipliers such as $n(F,E)$ and $v_D(F,E)$ (in the degenerated free carriers F-N approximation) are included in the constant C_{FN}, and B is a constant. In considering approximation, $n(F,E)$ can be found from

$$n_{3D}(F, E) = \frac{\sqrt{2}m_e^{\frac{3}{2}}}{\pi^2\hbar^3} \cdot \frac{\sqrt{E}}{1 + e^{\left(\frac{E-\mu}{k_B T_e(F)}\right)}}$$
$$n_{1D}(F, E) = \frac{m_e^{\frac{1}{2}}}{\sqrt{2}\pi\hbar d^2} \cdot \frac{1}{1 + e^{\left(\frac{E-\mu}{k_B T_e(F)}\right)}} \cdot \sum \frac{1}{\sqrt{E - E_{Ql}}}, \quad (9)$$

where $n_{3D}(F,E)$ and $n_{1D}(F,E)$ are the densities of available electrons for the bulk and quantum-size one-dimensional (1D) cases, respectively, E_{Ql} is the energy of the quantum confinement level, k_B is the Boltzmann constant, T_e is the electron temperature, d is the quantum structure diameter, and μ is the Fermi energy.

The distribution functions of density of states (D) and density of available electrons (n) for the 1D and three-dimensional (3D) cases are illustrated in Fig. 2. Quite different energy behavior of D and n is present for 1D and 3D cases. It is clear that the F-N slope change originates from $n(F,E)$, which is equal to the density of states multiplied by the Maxwell–Boltzmann carrier distribution, since the dependence of $v_D(F,E)$ becomes rather weak (nearly constant) at the high field region when considerable emission takes place [67,68].

In the following, the carrier heating by the applied electric field F is considered, where the hot carrier redistribution in the main and satellite valleys takes place. The effect of quantum confinement on the carrier distribution will also be shown.

First, the distribution of carrier density based on the Maxwell distribution has been analyzed. Contrary to the highly doped (degenerated) case, one can use the shifted Maxwell distribution for strong anisotropic and nondegenerated semiconductors. For low carrier concentration and nonelastic collisions, this assumption is quite reasonable and the following approximation holds:

$$\frac{p_0}{2m_e} \approx \frac{3}{2} k_B T_e(F),$$

where p_0 is the electron momentum, T_e is the effective temperature of carriers, and k_B is the Bolzman constant.

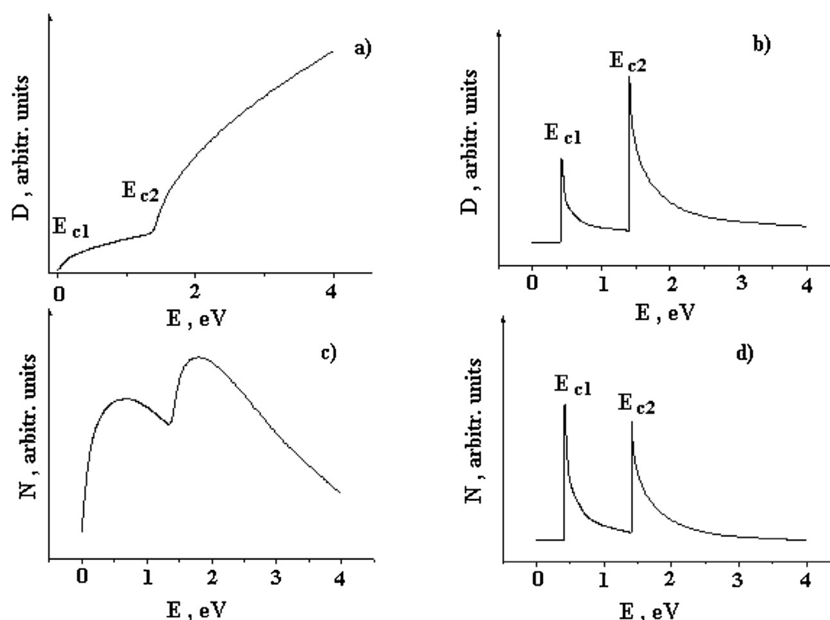

Fig. 2. Density of states (*D*) and density of carriers (*n*) as a function of the band energy for GaN main and satellite valleys in the case of 3D (*a*) and (*c*) and 1D (quantum confinement) structures (*b*) and (*d*): (a) density of states for bulk semiconductor (3D), (*b*) density of states for quantum states (1D), (*c*) density of carriers for bulk semiconductor (3D), and (*d*) density of carriers for quantum states (1D). (All curves were plotted for the electric field value 5×10^5 V/cm) [52].

In this case, the carrier distribution function can be found using the Maxwell approximation for $T_e(F)$ [69–73]:

$$f(p) = C \times \exp\{-(p - p_0)^2/2m_e k_B T_e(F)\}, \quad (10)$$

where p is the electron momentum, and p_0 is the unheated electron momentum.

When the carrier concentration equals to the ionized impurity concentration, one can use the following form of carrier distribution function [52]:

$$f_0(E) = C \times e\{-E/k_B T_e(F)\}, \quad (11)$$

where E is the energy of free electron, and F is the electric field.

2.1. Energy band reconstruction

In the case of nanostructures, the energy band of the material under consideration can be reconstructed based on the quantum-size confinement effect. Changing of the energy band parameters (energy bandgap, energy distance between main and satellite valleys, etc.) will influence the electron field emission significantly. Detailed analysis of energy band reconstruction of GaN due to the quantum-size confinement effect has been presented in [52]. A quantum oscillator approximation [71] has been used to estimate the possible influence of the quantum-size effects on the increase in the energy bandgap (which degrades the field emission efficiency due to the decreased free carrier concentration) and on the decrease in the electron affinity (which enhances the field emission). GaN has been used as a wide bandgap semiconductor material and the impact of the nanostructurization on the electronic properties has been considered. In the oscillator model, the heavy holes are considered as the nonmobile central particles, while electrons are represented as negatively charged spheres. In such a case, the solutions of the Schrödinger equation can be represented as Bessel functions with spherical symmetry. In the effective mass approximation the quantum dot (QD) electron spectra can be obtained from the Schrödinger equation with spherical potential *U (r)* and finite band barriers (due to offsets of conduction and valence bands at semiconductor-vacuum interface). The eigenvalues of energy are obtained from the Schrödinger equation. The energy difference

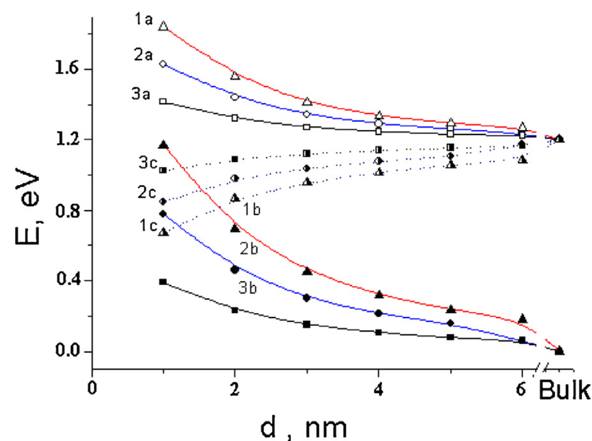

Fig. 3. Calculated energy shift of satellite valley (*a*), main valley (*b*), and intervalley energy difference (*c*) in GaN due to the quantum confinement effect: zero-dimensional case (*1a–1c*), 1D case (*2a–2c*), and two-dimensional case (*3a–3c*) [52].

between the $E_0(X)$ and $E_0(\Gamma)$ conductance band minima is about 1.19 eV [55] for the bulk GaN material and continuously decreases down to 0.6 eV with decreasing QD size d. In Fig. 3, one can see the calculated curves which illustrate the band transformation due to quantum confinement effects. The increasing of energy bandgaps for main (k-space point Γ) and satellite (k-space point X) valleys has been observed with decreasing nanotip diameter $d < 10$ nm. Due to lower electron effective mass in main valley, the growth of $E_g(\Gamma)$ is higher than $E_g(X)$. As a result, the intervalley energy difference decreases with the decrease in nanotip diameter (Fig. 3).

The solution of the Schrödinger equation in the case of spherical symmetry corresponds to spherical Bessel functions (J, N):

$$\Psi_1 = BJ(k, r) \quad (12)$$

(inside the QD),

$$\Psi_2 = AN(\beta, r) \quad (13)$$

(outside the QD), with

$$\beta = \frac{\sqrt{2m^*_{e2}(V(r)-E)}}{\hbar}, \quad k = \frac{\sqrt{2m^*_{e1}E}}{\hbar}, \tag{14}$$

where m^*_{e1} and m^*_{e2} are the effective masses of electrons inside and outside of the QD, respectively, A and B are constants which define the magnitude of wave function, and E is the eigenvalue of energy for ground s-orbital state.

Using boundary and initial conditions such as

$$\Psi_1(d/2) = \Psi_2(d/2), \tag{15}$$

$$\frac{1}{m^*_{e,1}}\frac{d\Psi_1(d/2)}{dr} = \frac{1}{m^*_{e,2}}\frac{d\Psi_2(d/2)}{dr}, \tag{16}$$

one obtains the following non-algebraic equation:

$$\frac{\frac{d\beta}{2}-1}{m^*_{e,2}} = \frac{1-\frac{dk}{2}\cot(\frac{kd}{2})}{m^*_{e,1}}. \tag{17}$$

The solution of Eq. (17) provides the electron energy levels. A similar relation takes place for holes (with effective masses of m^*_{h1}, m^*_{h2}). To determine the constants A and B [Eqs. (12) and (13)], it is necessary to use the normalization requirement:

$$\int_0^\infty |\Psi|^2 dr = 1,$$

which is typical for single electron approximation.

Calculations have been performed for the energy band reconstruction of nanometer size objects in the presence of the quantum-size confinement effect. The calculation shows a decrease in the energy difference between the main and satellite valleys (Fig. 3). This enhances the possibility of an intervalley electron transfer effect during field emission.

2.2. Comparison of the theory with experiment results

The GaN structure used in experiments was grown by low-pressure MOCVD on (0001) c-plane sapphire using a modified EMCORE GS-3200 system with trimethylgallium (TMGa) and ammonia (NH_3) as source materials. A buffer layer of about 25-nm-thick GaN was first grown at 510 °C on sapphire. The structure used is a single 1.5-µm-thick n-GaN layer ($n = 2 \times 10^{17}$ cm^{-3}). It was grown at the temperature 1100 °C. A patterned Ti mask served to provide electrical contact to the sample as well an etch mask. The Ti metal contacts were unannealed. Quantum nanostructures were formed by photoelectrochemical etching of GaN [74]. With an additional current and under process-specific conditions it produced high etch selectivity at the dislocations. Photoelectrochemical etching of GaN is a means of greatly improving the chemical reactivity of GaN at room temperature. Ultraviolet illumination generates electron–hole pairs at the semiconductor surface, which enhance the oxidation and reduction reactions within an electrochemical cell. The GaN layer with quantum dots shown in Fig. 4 was etched for 6 min in a stirred 0.1 M KOH solution using Hg lamp illumination and a 1 mA current source.

At the beginning the electric field enhancement coefficient due to geometry of tips (see Fig. 4) has been determined $\beta^* \approx 30$. The electric field enhancement coefficient was calculated by using the floating sphere model according to equation $\beta^* \approx h/r + 3$, where h is the tip height and r is the radius curvature of the tip [75].

Consideration of the above analyzed mechanisms allowed the calculation of the current-voltage characteristics I–V of the EFE for GaN. The corresponding F-N plots are shown in Fig. 5. The F-N curves for nanostructured (1D) and bulk (3D) materials are quite different. Such behaviour can be explained by peculiarities of electron intervalley redistribution (Fig. 6). In contrast to quantum-size cathodes (1D), with almost full intervalley carrier redistribution (Fig. 6) above the threshold field, the bulk (3D) wide bandgap material shows different characteristics. The electron redistribution for GaN ($r = n_\Gamma/(n_\Gamma + n_X)$) has not exceed 60% (Fig. 6). Thus the total number of carriers is constant, but when the field is increased the

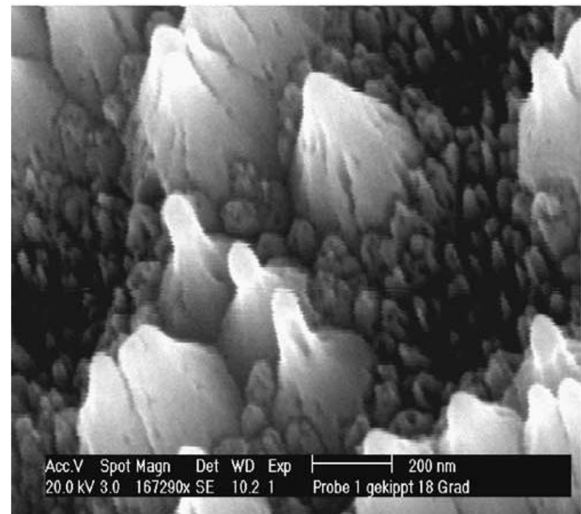

Fig. 4. SEM micrograph of a photoelectrochemical etched GaN surface.

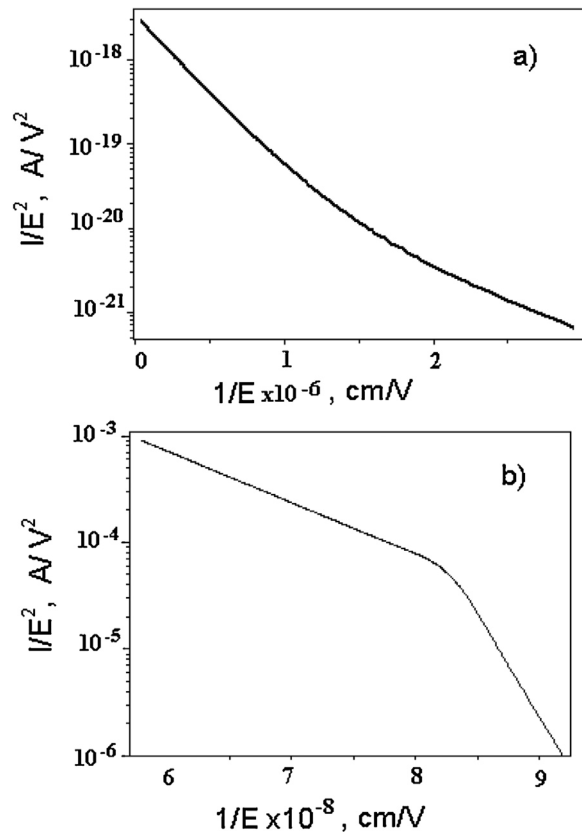

Fig. 5. Comparison of FE currents for bulk GaN surface (a) and 1D GaN nanotextured surface (b). Differences in the slope change originate from differences in density of states for bulk and nanotextured many valley semiconductors [52].

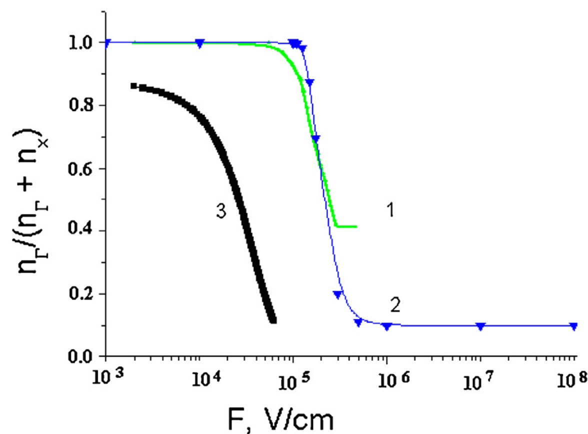

Fig. 6. Comparison of the intervalley redistribution of electrons for GaN with large intervalley distance (1), GaN with quantum-size confinement (2), and GaAs with small intervalley distance (3). (n_Γ is the electron concentration in the main Γ valley, and n_X is the electron concentration in the satellite valley).

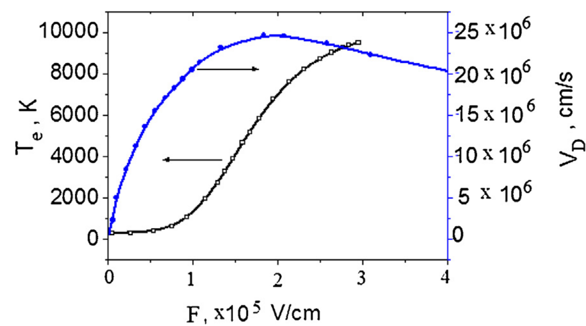

Fig. 7. Drift velocity and electron temperature in GaN bulk material as functions of the electric field [67].

carrier energy increases and electron transfer effect takes place. The values n_Γ and n_X have been calculated according to equations:

$$n_\Gamma(F) = \int_{E_{C1}}^{E_{C2}} N(E, F)dE, \tag{18}$$

$$n_X(F) = \int_{E_{C2}}^{\chi_0} N(E, F)dE, \tag{19}$$

where n_Γ is the total amount of carriers in the energetic band between E_{C1} and E_{C2} (in the main valley), n_X is the total amount of carriers in energetic band between E_{C2} and vacuum (in the satellite valley), and $N(E,F)$ is the carrier density distribution.

Therefore, the resulting current consists of two (number of active valleys) parallel currents, which depend on F in a rather different manner. Each of them can be described by the F-N equation for small electric field changes.

The total field emission current is the sum of two currents from the main and satellite valleys $J = J_{C2} + J_{C1}$ [(see Eq. (7)]. Therefore, the F-N relation is a very rough approximation in case of multivalley semiconductors, which is only valid for the case of low fields.

The calculated curves in F-N scale (Fig. 5) were compared with experimental field emission currents (Fig. 1) over a wide field range. The experimental samples had a nanotextured surface [52]. The experimental curves manifested unique peculiarities (slope change, etc.) but could be described well by the extended modified F-N theory; this theory includes the quantum confinement effects on the nanotextured sample surface and nondegenerated statistics for hot carriers. It is clear that the intervalley redistribution becomes remarkable when the energy of hot carriers reaches the intervalley energy difference of ΔE. Fig. 6 illustrates the intervalley redistribution of electrons in GaAs with small intervalley difference, GaN with large intervalley difference, and GaN with quantum-size tips. In the case of GaN cathodes, the intervalley redistribution occurs at significantly higher electric fields (>1 × 10^5 V/cm). An important result is also that for quantum-size GaN emitters, almost all carriers transit into the satellite valley at high electric field, while for bulk GaN emitters, a significant part of carriers is left in the main valley, even at very high fields.

The calculated drift velocity [52] and the electron temperature are shown in Fig. 7 as functions of the electric field and correspond to the result in Ref. [67]. Indeed the field dependence of electron temperature causes the intervalley electron redistribution [54,60,61].

It should be mentioned that the curve with a smaller slope at higher electric fields was obtained only for quantum-sized cathodes (Fig. 5). In the case of bulk emitter, a concave curve with larger slope at higher electric fields was observed (Fig. 5(*a*)). Using Fig. 5(*a*) the calculation for bulk emitter has shown saturated carrier redistribution at very high fields with maximum carrier fraction of about 60% in the satellite valley (see Fig. 6). Whereas in the case of quantum size emitters [(Fig. 5(*b*)], sharp and complete carrier redistribution must take place.

The field emission *I–V* characteristics in F-N coordinates (Fig. 5) were calculated according to Eq. (4), with taking into account the energy (Fig. 2) and field (Fig. 6) intervalley electron redistribution for 3D and 1D cases.

Taking into consideration the higher mobility for the main valley, it is clear that for the bulk emitter the current from the upper valley never becomes dominant at high fields. For bulk emitter, the emission starts from the main valley at low fields, with extremely small currents (practically undetectable). At moderate fields, the carrier distribution demonstrates remarkable concentration in the satellite valley. Here, the slope of the F-N characteristics is determined by the satellite valley work function. In the region of the highest electric fields, the main valley begins to play an important role because of the increased probability of tunneling through the emission barrier and high electron concentration. The slope in the F-N curve increases again (Fig. 5(*a*)).

In the case of quantum-size cathodes, the experimental curve in Fig. 1 corresponds to electron emission from the main valley (at low electric field; before the slope changing point) and from the satellite valley (at moderate fields; beyond the slope changing point) with two different slopes. The current from the main valley becomes negligible beyond the slope changing point. At moderate fields, most of the carriers are transferred into the satellite valley (Fig. 6). As a result, the slope of the F-N curve is decreased and determined by the work function of the satellite valley [(Fig. 5(*b*)].

The reason for the slope change in GaN compared with GaAs cathodes is the following: in GaAs the carriers are already heated before field emission, demonstrating remarkably high currents. As a result, the slope changes are not seen in the field emission characteristic for a GaAs emitter. The slope change in the case of emission from GaN nanostructured surfaces is a good evidence of the quantum confinement effect on nanosized cathodes.

The calculated and experimental F-N curves are shown together for comparison in Fig. 8. Different calculated curves in Fig. 8 correspond to different intervalley distances. The quantum-size effect decreases the intervalley energy differences ΔE (see Fig. 3). The theoretical and experimental curves are practically coincident for ΔE = 0.8 eV (Fig. 8, curves 1 and 4). The sharp current increase at low electric fields for a small intervalley distance in GaN (Fig. 8, curve 2) is caused by easier intervalley carrier redistribution and low work function of the quantum-sized cathode.

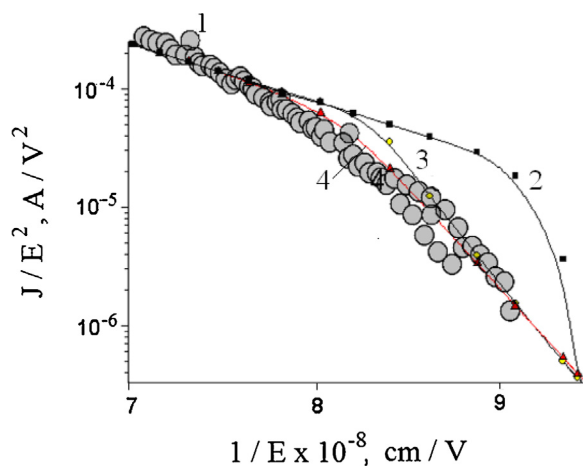

Fig. 8. *I–V* characteristics of the field emission current (in F-N scale): Experimental results (1), calculated curves for the intervalley distance of 0.5 eV (2), 0.7 eV (3), and 0.8 eV (4) [52].

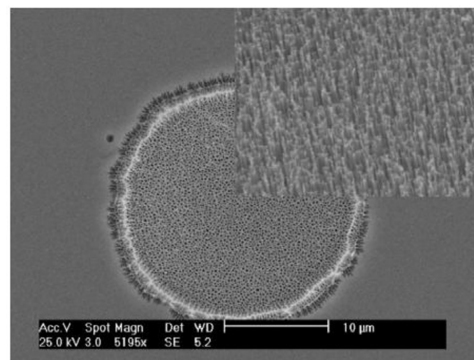

Fig. 9. SEM image of the argon plasma (20 min) and PEC (12 min) etched GaN rods. Only n^+-GaN mesa region is affected. On the top right side is the side view of the GaN rods [59].

The difference in the slope values in the F-N plot can be used for intervalley distance estimation. Large heating of the free electrons and interband electron redistribution take place in the studied GaN field emitter with nanostructured surface.

3. Photo-field emission from GaN nanorods

GaN is a promising material for high-frequency, high-power, and high-temperature electrical and optical ultraviolet devices due to its unique material parameters [76,77]. It is very important to know the precise band structure of GaN. Many groups have theoretically calculated the band structure for GaN [78,79] and measured some characteristic values in it, e.g., the intervalley energy distance [60,80–82]. But until now, there have been different calculated and measured values for the GaN energy-band parameters, including the difference between the main Γ and the satellite valley.

There are several methods for studying of the energy-band structure of materials. The first method to determine the electronic-band structure for semiconductors is the electroreflectance (ER) modulation spectroscopy due to its high resolution and its sensitivity with small changes in band structure. The ER modulation spectroscopy method is based on electromodulation, in which reflection spectra are studied [83]. Wide application of this method is complicated due to the requirement that the electric field must be uniform at the space-charge region. The second method is inverse photoemission spectroscopy (IPES) [84]. IPES is a surface-science technique used to study the unoccupied electronic states, structure of surfaces, thin films, and adsorbates. In case of IPES investigations, a well-collimated beam of electrons with energy less than 20 eV is directed to the sample. Due to low energy of incident electrons, their penetration depth is only several atomic layers. The studies of a field-emission energy distribution also give information about electronic states that lie within the Fermi energy [85–87]. The ultraviolet photoelectron spectroscopy method allows one to determine the electron affinity of III-nitrides and their alloys [62]. Photofield-emission spectroscopy is also used for the characterization of the energy-band structure [88]. Several authors have discussed the possibility of investigating the electron states between the Fermi and vacuum levels by studying the field emission of optically excited electrons [89,90]. This method is based on the work function change under photoexcitation of electrons at their tunneling through a barrier according to the Fowler-Nordheim mechanism. A spectroscopy of the GaN band structure will be possible for field-emission measurements with monochromatic illumination of the depleted emitter tips.

The investigation of the photon-assisted field emission from GaN nanorods and determination of some energy band structure parameters have be performed in [54,91]. The GaN field-emitter rods were fabricated on a wafer with n-GaN active layer (5 µm) sandwiched between n^+-GaN cap layer (100 nm) and 300 µm thick n^+-GaN substrate. The active layer and top layer were grown with metal-organic chemical vapor deposition using a standard method. A photoresistant mask was used for the argon plasma etching (Ar flow of 20 sccm, background pressure of 50 mtorr, and *rf* power of 300 W) of a circular mesa with 400 nm height. Afterwards, the samples were cleaned in acetone and photoelectrochemically (PEC) etched [74] in KOH. UV illumination generates electron-hole pairs at the n^+-GaN surface, which enhance the oxidation and reduction reactions taking place in the electrochemical cell, formed by immersing the substrate in a 0.1 *M* KOH stirred solution. This allows one to achieve selectivity in etching n^+-GaN with respect to n-GaN. The GaN sample was PEC etched for 12 min in the presence of Hg lamp illumination. The scanning electron microscope (SEM) image of GaN nanorods after PEC etching is shown in Fig. 9. Further etching up to 38 min increased the height of the rods by extending them into the n-GaN layer below the n^+-GaN cap. The n-GaN material around the mesa was not affected by this step and remained unetched. The selectivity in etching the area containing the nanorods but not the surrounding area is due to the presence of the thin n^+-GaN layer in the "nanorod area", which promotes PEC etching. An Ohmic-contact cathode electrode was formed on the back side of the n^+-GaN substrate, while an indium tin oxide (ITO) coated quartz glass was used as the anode electrode. The distance between the GaN emitter and ITO anode was controlled by the 7.5 or 20 µm thick Kapton spacer disk with 1 mm hole diameter. The light was focused onto the field emitter in a high-vacuum chamber through the quartz glass from inside or outside the positioned laser or LED. LEDs were connected to the anode side for illuminating the sample during FE measurements (Fig. 10). Laser diodes with different wavelengths, namely, infrared (IR) ($\lambda \approx 880$ nm, P = 5 mW), red (R) ($\lambda \approx 650$ nm, $P = 5$ mW), green (G) ($\lambda \approx 532$ nm, $P = 5$ mW), and ultraviolet (UV) ($\lambda \approx 365$ nm, $P = 110$ mW) were used for the photoassisted field emission. The vacuum achieved in the FE setup used for the characterization was $\sim 2 \times 10^{-8}$ mbar.

The experimental electron-field-emission curve in the Fowler–Nordheim coordinates (*lg* I/V^2-$1/V$) has two different slopes, namely, a lower slope at low voltages and a higher slope at high voltages [(Fig. 11(*a*)]. The voltage of the slope change is equal to 670 V, which corresponds to a macroscopic electric field of 8.9×10^5 V/cm. The effective electron affinities (barriers for

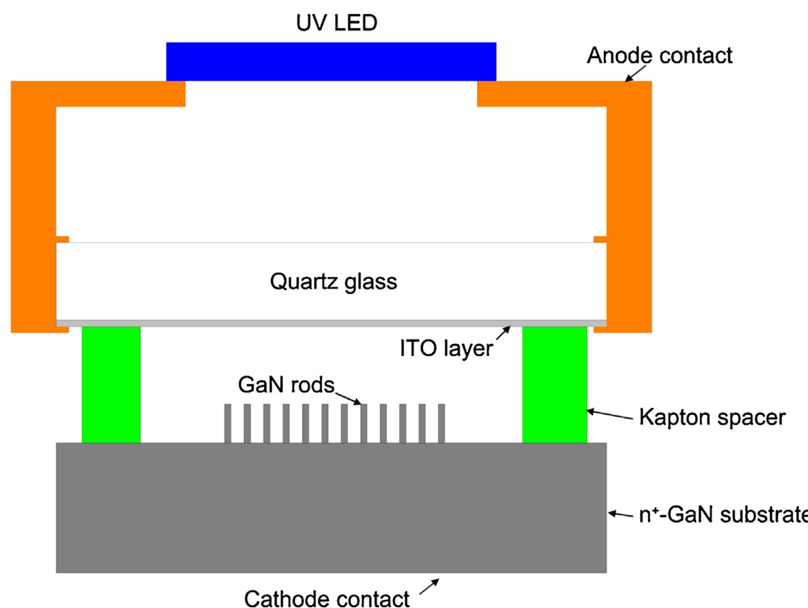

Fig. 10. Biasing scheme of the GaN rods for photoexcited FE spectroscopy in the vacuum chamber [59].

electron tunneling at field emission) have been determined from the slopes of the F-N plot,

$$\chi_{ef} = \chi/\beta^{2/3}, \quad (20)$$

where χ is the electron affinity and β is the electric field enhancement coefficient.

The ratio of $\chi_1/\chi_2 = \chi_{1ef}/\chi_{2ef}$ is equal to 2.07. This is in good agreement with the ratio of electron affinities of the GaN Γ valley (3.3 eV) and the X valley (2.21 eV) [62,81] if we take into account the energy barrier lowering due to Schottky effect ($\Delta\Phi \approx 1.1$ eV).

The electron-field emission from the upper X valley dominates in the low-voltage region. The electric field in GaN is high enough to heat some of the electrons and transfer them from the Γ valley into the X valley. Because the X-valley electrons go through a lower and thinner vacuum barrier (high tunneling probability), their contribution to emission current dominates. But following the growth of voltage and corresponding lowering and thinning of the energy barrier due to the Schottky effect, the influence of Γ-valley electrons is increased. These processes were theoretically described in Ref. [52].

During the investigation of the photofield emission, the influence of illumination on the emission current was observed only in the low-voltage region of the curve. The experimental curves in F-N coordinates without and with illumination were similar in the high-voltage region.

3.1. IR irradiation

The experimental field and photofield emission curves at IR illumination are shown in Figs. Fig. 11(*b*) and (*b*'). The increase in emission current (1.8 times) and decrease in the curve slope were observed. Under IR illumination, the change of the emission curve slope was at lower voltage ($V = 554$ V, $E_{th} = 7.4 = 10^5$ V/cm). The effective electron affinities were determined from the slopes of the F-N plot measured without (Fig. 11(*b*'), curve 1) and with IR illumination (Fig. 11(*b*'), curve 2). The IR light excited the electrons from the bottom of the Γ-valley. Excited electrons gave significant influence on the emission current. The comparison of experimental curve slopes without and with illumination allowed to estimate the energy barrier of IR light-excited tunneling electrons as $\Phi_{IR} = 1.34$ eV (taking into account a Schottky barrier lowering of $\Delta\Phi = 0.56$ eV). The difference of the Γ- valley electron affinity and the energy barrier of IR light-excited electrons was 1.40 eV, which practically coincided with the energy of the IR photon ($h\nu = 1.41$ eV). In this case, the subbandgap transitions (inner band electron transitions) caused by photon adsorption were realized. The adsorption coefficient due to subbandgap transitions in GaN increased with the photon energy.

3.2. Green light irradiation

Fowler–Nordheim plots before and under G light illumination are shown in Fig. 11(*c*). In the case of green-light illumination ($h\nu_G = 2.25$ eV), the sum of $\Phi_G + h\nu_G$ is noticeably higher (3.8–4.0 eV versus $\Phi_\Gamma = 3.3$ eV), where Φ_G is the energy barrier of green light-excited tunneling electrons determined from experiment. This indicates a partial electron thermalization before the field emission took place.

During electron-field emission from GaN mesa without PEC etching, an increase of the current due to G light illumination was also observed. On the other hand, R light had small influence on emission. This fact could be explained by the lower R light-absorption coefficient in GaN. Some other peculiarities were obtained for photofield emission from the GaN mesa (without PEC etching). One such peculiarity was the sharp growth of the current at a determined voltage (sharp conditioning). The maximum applied voltage was successively increased with initial emission 550 V. The macroscopic-threshold electric field for a cathode-anode distance of 20 µm was 2.75×10^5 V/cm. After the sharp conditioning at 800 V, the G light influence disappeared. The possible reason of this effect may be caused by desorption of atoms and molecules from the surface of the tips. As a result the effective work function is decreased due to removing the influence of positive dipoles on the surface. Another peculiarity of the photofield emission was the memory effect. The electron-field emission curves were practically coincided in subsequent measurements. At R light illumination, a small growth in current was observed. The subsequent measured curves without illumination showed equal results. Further measurements at G light illumination demonstrated an increase in the emission-current with similar values for the subsequent measurements without illumination. During R light illumination there was the partial desorption of atoms and molecules from the surface of

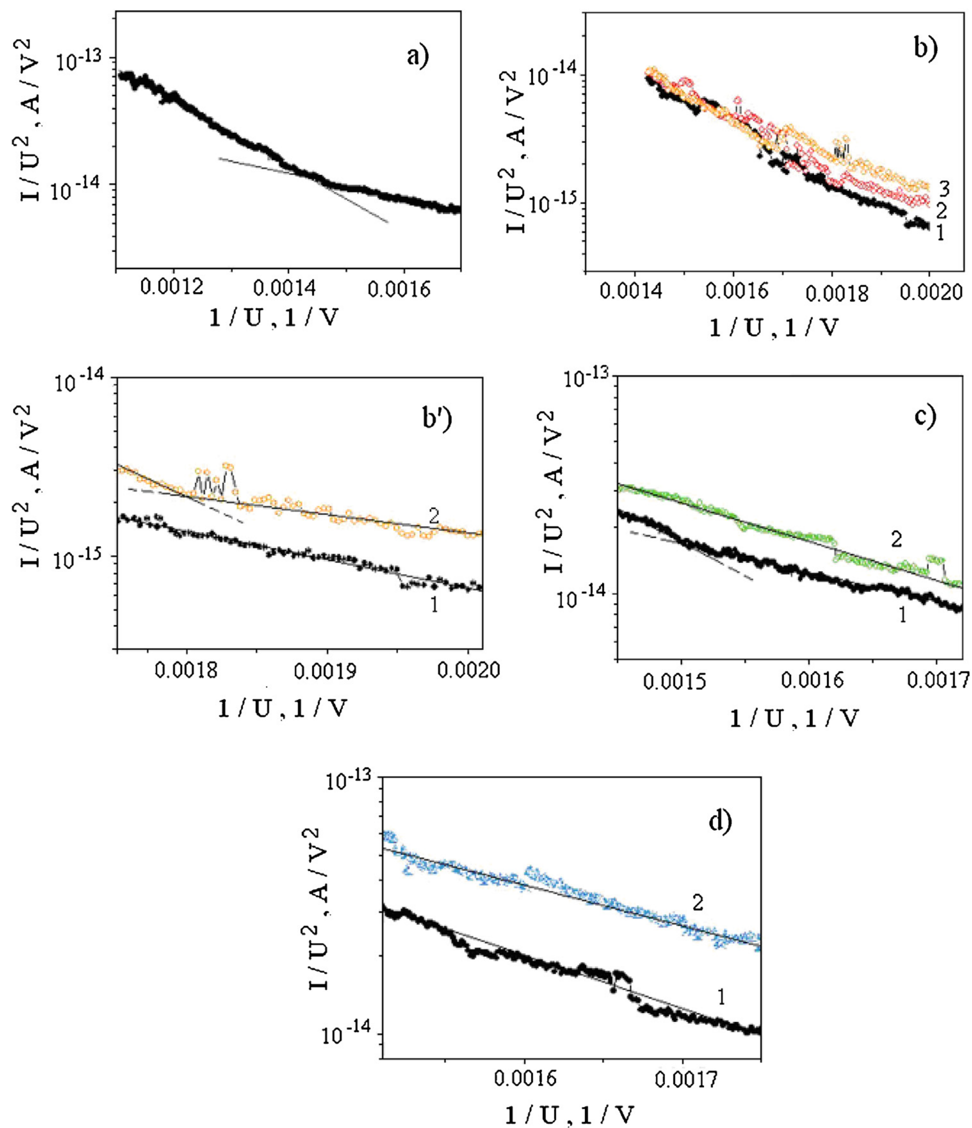

Fig. 11. Fowler–Nordheim plots of the electron field and photofield emission from nanostructured GaN rods: (*a*) F–N curve without illumination; (*b*) and (*b*') without and with IR light illumination (in different scales); (*c*) without and with G light illumination; (*d*) without and with UV light illumination: (1 without illumination; 2 and 3 under illumination) [91].

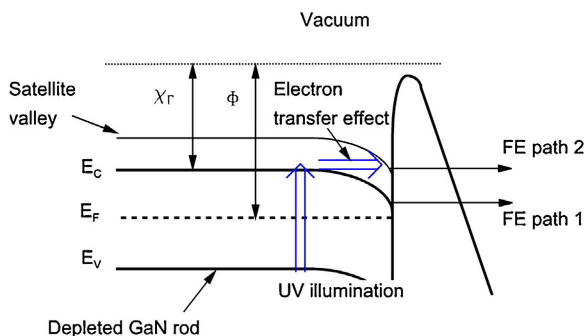

Fig. 12. Energy band diagram of a depleted GaN rod and FE path from the Γ valley (FE path 1, electron affinity χ_{Γ}) and from the satellite valley (FE path 2, $\chi_X < \chi_{\Gamma}$) without and with UV illumination, respectively. The applied field penetrates into the GaN rod with $E > 150$ kV/cm [59].

the tips. Subsequent illumination with G light causes additional desorption of the atoms and molecules. After that the emission current is the same as during illumination.

3.3. UV irradiation

The initial FE current was set to several nanoamperes. Upon emitter illumination, the current increased immediately and then fluctuated around a value, which was up to one order of magnitude higher than the initial current. Additional electron-hole pairs were generated by absorption of UV photons with energies larger than the bandgap of the GaN nanorods (3.4 eV). Electrons reached the surface quickly due to the small diameter of the GaN nanorods. The field necessary for FE penetrated into the depleted GaN rod (electrical field $E > E_{th} = 150$ kV/cm) and enabled electron transfer from the Γ valley to the satellite valleys. The photoexcited electrons contributed to the FE process from the satellite valley due to their smaller electron affinity χ (Fig. 12). The electron FE current shown in the F-N plot (Fig. 13) clearly demonstrates two different slopes for nonilluminated and UV illuminated emissions. In the case where the GaN rods are not illuminated, the emitter is almost depleted and emission takes place from the Γ valley ($\chi = 3.3$ eV).

Upon UV illumination, new electrons are generated from the valence band and they occupy the upper valley. The main emission occurs from this valley, which has lower electron affinity. The pres-

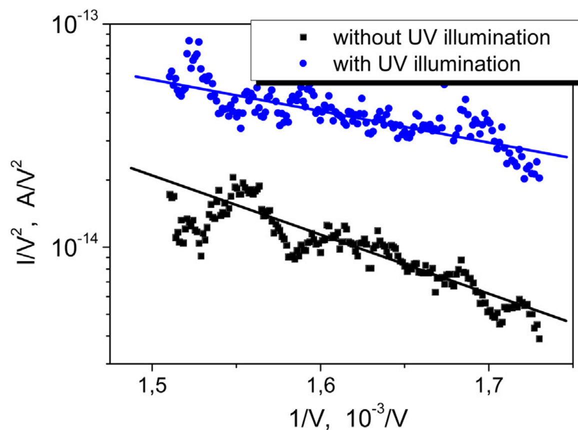

Fig. 13. F-N plots of the electron FE from nanostructured GaN rods. The slope decreases under UV illumination [59].

ence of a high electric field in the emitter tip supports the presence of the electron transfer effect. The electron affinity difference (equal to the energy difference between the valleys) can also be calculated by evaluating the two slopes m of the F-N characteristic.

$$m = -2.84 \times 10^7(\Phi^{3/2}/\beta). \quad (21)$$

Correct estimation of the field enhancement coefficient β is difficult to be made from the scanning electron microscopy (SEM) image of nanostructured surfaces and so is the calculation of the absolute value of the real work function Φ. The ratio of Φ_1/Φ_2 (work function for Γ valley/work function for the satellite valley) can, however, be determined from the two emission F-N curves (Fig. 13) with the same β

$$\Phi_1/\Phi_2 = \chi_\Gamma/\chi_X = (m_1/\mathrm{m}_2)^{2/3} \quad (22)$$

The obtained value of $\chi_\Gamma/\chi_X = 1.53$ (GaN rod) can be used to calculate χ_X for given values of χ_Γ, i.e. $\chi_\Gamma = 3.3$ eV. The calculated energy difference between the valleys $\Delta E = 1.15$ eV is in good agreement with the values published in [81] ($\Delta E = 1.1$ eV). The UV illumination and the presence of a high electric field in the emitter tip permit the manifestation of the electron transfer effect in the GaN field emitter structure, leading to the change in the emission characteristics. The current from the upper valley becomes dominant at a rather small electron concentration n in the upper valley due to much smaller electron affinity in this valley, as compared to the Γ valley.

4. Conclusions

The small electron affinity of wide gap structures opened a new way for realizing effective electron field emitters, especially when combined with nano-dimensional features offered, for example by nanowires. Structures with a quantized band spectrum have important features of optical, electric etc. properties. Special attention is paid to semiconductor structures with a many-valley band spectrum, where the quantization provides the electron field emission from upper satellite valleys with a relatively low work function. The equilibrium electron population of these bands in low-strength electric fields is very low, but electron emission will be facilitated by the decreasing of the distance of these bands from the main conduction band, by the specific energy distribution of the electron states and, even more effective, by heating of the free electrons due to the dimensional quantization. In addition, the energy of the main conduction band gradually rises to vacuum (free electron) level, where the field emission starts even at low fields due to the decreasing of the work function. The fundamental factor for quantum cathodes is the decreasing of the inter valley energy distance due to the size quantization from $\Delta E = E_{C2} - E_{C1} = 1.3$ eV to 0.6 eV for quantum dot cathode of GaN, i.e., more than two times. Other positive factor is the multi tips structure, which determines the enough large electron emission current from the unit of the cathode area.

Photo-assisted field-emission experiments on various wide bandgap semiconductor materials allowed a systematic study of the material properties including details of their band structure. Nanowires were studied using various semiconductors such as III-N (GaN). This allowed an in-depth study of their energy band diagram such as electron affinities and satellite valley positions. The quantum confinement effect strongly changed the energy band diagram of nanostructures and consequently, the main physical properties of the materials of which they were made. 1D and 0D structures of semiconductors are ideally suited for the realization of devices for high-speed/high-frequency.

Acknowledgements

We want to acknowledge Dr. O. Yilmazoglu and Prof. H. Hartnagel from Technical University of Darmstadt (Germany) for fruitful discussion and collaboration.

References

[1] H. Morkoc, Handbook of Nitride Semiconductors and Devices, Vol. 3, WILEY-VCH Verlag GmbH & Co. KGaA, Weinheim, 2009 (ISBN: 978-3-527-40839-9).
[2] B. Gelmont, K. Kim, M. Shur, Monte Carlo simulation of electron transport in gallium nitride, J. Appl. Phys. 74 (1818) (1993).
[3] S.C. Jain, M. Willander, J. Narayan, R. van Overstraeten, III–nitrides: growth, characterization, and properties, J. Appl. Phys. 87 (965) (2000).
[4] B.K. Ridley, Exact electron momentum-relaxation times in GaN associated with scattering by polar-optical phonons, J. Appl. Phys. 84 (1998) 4020–4021.
[5] U.V. Bhapkar, M.S. Shur, Monte Carlo calculation of velocity-field characteristics of wurtzite GaN, J. Appl. Phys. 82 (1649) (1997).
[6] J. Kolnik, I.H. Oguzman, K.F. Brennan, Electronic transport studies of bulk zincblende and wurtzite phases of GaN based on an ensemble Monte Carlo calculation including a full zone band structure, J. Appl. Phys. 78 (1995) 1033.
[7] H. Morkoc, Beyond SiC! III–V nitride based heterostructures and devices, in: Y.S. Park (Ed.), SiC Materials and Devices, Vol. 52, Academic Press, 1998, pp. 307–394, Willardson and Beer Series, (series eds R.K. Willardson and A.C. Beer) Chapter 8.
[8] M.-C. Lin, K.-H. Huang, P.-S. Lu, P.-Y. Lin, R.F. Jao, Field-emission based vacuum device for the generation of terahertz waves, J. Vac. Sci. Technol. B 23 (2005) 849.
[9] I. Brodie, C.A. Spindt, Vacuum microelectronics, in: P.W. Hawkes (Ed.), Advances in Electronics and Electron Physics, 83, Academic Press, New York, 1992, pp. 1–106.
[10] K. Yokoo, Functional field emission for high frequency wave application, in: Technical Digest of IVMC 99, 1999, pp. 206–220 (Darmstadt, Germany).
[11] O. Yilmazoglu, H. Mimura, K. Mutamba, H. Hartnagel, K. Okamura, H. Shimawaki, K. Yokoo, Generation of a bunched electron beam by field-emitter structures, in: ITG Proc. 165, Conference on Displays and Vacuum Electronics, Garmisch-Partenkirchen, Germany, (May 2001), 2001, pp. 263–267.
[12] E.G. Zaidman, M.A. Kodis, Emission gated device issues, IEEE Trans. Elec. Dev. 38 (1991) 2221.
[13] D.R. Whaley, B.M. Gannon, C.R. Smith, C.M. Armstrong, C.A. Spindt, Application of field emitter arrays to microwave power amplifiers, IEEE Trans. Plasma Sci. 28 (2000) 727.
[14] X. Duan, Y. Huang, Y. Cui, J. Wang, C.M. Lieber, Indium phosphide nanowires as building blocks for nanoscale electronic and optoelectronic devices, Nature 409 (2001) 66.
[15] W.Q. Han, S.S. Fan, Q.Q. Li, Y.D. Hu, Synthesis of gallium nitride nanorods through a carbon nanotube-confined reaction, Science 277 (1997) 1287.
[16] H. Yoshida, T. Urushido, H. Miyake, K. Hiramatsu, Formation of GaN self-organized nanotips by reactive ion etching, Jpn. J. Appl. Phys. 40 (2001) L1301.
[17] J.L. Shaw, H.F. Gray, K.L. Jensen, T.M. Jung, Graded electron affinity electron source, J. Vac. Sci. Technol. B 14 (1996) 2072.
[18] T. Sugino, T. Hori, C. Kimura, T. Yamamoto, Field emission from GaN surfaces roughened by hydrogen plasma treatment, Appl. Phys. Lett. 78 (2001) 3229.
[19] R.J. Nemanich, M.C. Benjamin, S.P. Bozeman, M.D. Bremser, S.W. King, B.L. Ward, R.F. Davis, B. Chen, Z. Zhang, J. Bernhole, Negative electron affinity of AlN and AlGaN alloys, Mater. Res. Soc. Symp. Proc. 395 (1996) 777.
[20] J.I. Pankove, H. Schade, Photoemission from GaN, Appl. Phys. Lett. 25 (1974) 53.

[21] W. Czarczynski, S. Lasisz, M. Moraw, R. Paszkiewicz, M. Tlaczala, Z. Znamirowski, Field emission from GaN deposited on the (100) Si substrate, Appl. Surf. Sci. 151 (1999) 63.
[22] I. Berishev, A. Bensaoula, A. Rusakova, M. Karabutov Uagarov, V.P. Ageev, Field emission properties of GaN films on Si(111), Appl. Phys. Lett. 73 (1808) (1998).
[23] B.L. Ward, O.-H. Nam, J.D. Hartman, S.L. English, B.L. McCarson, R. Schlesser, Z. Sitar, R.F. Davis, R.J. Nemanich, Electron emission characteristics of GaN pyramid arrays grown via organometallic vapor phase epitaxy, J. Appl. Phys. 84 (5238) (1998).
[24] B. Liu, Y. Bando, C. Tang, F. Xu, J. Hu, D. Golberg, Needlelike bicrystalline GaN nanowires with excellent field emission properties, J. Phys. Chem. B 109 (2005) 17082.
[25] D.K.T. Ng, M.H. Hong, L.S. Tan, Y.W. Zhu, C.H. Sow, Field emission enhancement from patterned gallium nitride nanowires, Nanotechnology 18 (2007) 375707.
[26] C.C. Chen, C.C. Yeh, C.H. Chen, M.Y. Yu, H.L. Liu, J.J. Wu, K.-H. Chen, L.-C. Chen, J.-Y. Peng, Y.-F. Chen, Catalytic growth and characterization of gallium nitride nanowires, J. Am. Chem. Soc. 123 (2001) 2791.
[27] X. Xiang, H. Zhu, One-dimensional gallium nitride micro/nanostructures synthesized by a space-confined growth technique, Appl. Phys. A 87 (2007) 651.
[28] Z. Chen, C.B. Cao, W.S. Li, C. Surya, Well-aligned single-crystalline GaN nanocolumns and their field emission properties, Cryst. Growth Des. 9 (2009) 792.
[29] G.S. Cheng, L.D. Zhang, Y. Zhu, G.T. Fei, L. Li, C.M. Mo, Y.Q. Mao, Large-scale synthesis of single crystalline gallium nitride nanowires, Appl. Phys. Lett. 75 (1999) 2455.
[30] Z. Liliental-Weber, Y. Chen, S. Ruvimov, J. Washburn, Formation mechanism of nanotubes in GaN, Phys. Rev. Lett. 79 (1997) 2835.
[31] J.Y. Li, Z.Y. Qiao, X.L. Chen, Y.G. Cao, Y.C. Lan, C.Y. Wang, Morphologies of GaN one-dimensional materials, Appl. Phys. A 71 (2000) 587.
[32] S.Y. Bae, H.W. Seo, J. Park, H. Yang, J.C. Park, S.Y. Lee, Single-crystalline gallium nitride nanobelts, Appl. Phys. Lett. 81 (2002) 126.
[33] J. Su, G. Cui, M. Gherasimova, H. Tsukamoto, J. Han, D. Ciuparu, S. Lim, L. Pfefferle, Y. He, A.V. Nurmikko, C. Broadbridge, A. Lehman, Catalytic growth of group III-nitride nanowires and nanostructures by metalorganic chemical vapor deposition, Appl. Phys. Lett. 86 (2005) 013105.
[34] S. Gupta, H. Kang, M. Strassburg, A. Asghar, M. Kane, W.E. Fenwick, N. Dietz, I.T. Ferguson, A nucleation study of group III-nitride multifunctional nanostructures, J. Cryst. Growth 287 (2006) 596.
[35] G. Nabi, C. Cao, W.S. Khan, S. Hussain, Z. Usman, M. Safdar, S.H. Shah, N.A.D. Khattak, Synthesis, characterization, growth mechanism, photoluminescence and field emission properties of novel dandelion-like gallium nitride, Appl. Surf. Sci. 257 (2011) 10289.
[36] B. Liu, Y. Bando, C. Tang, F. Xu, D. Golberg, Quasi-aligned single-crystalline GaN nanowire arrays, Appl. Phys. Lett. 87 (2005) 073106.
[37] B. Ha, S.H. Seo, J.H. Cho, C.S. Yoon, J. Yoo, G.C. Yi, C.Y. Park, C.J. Lee, Optical and field emission properties of thin single-crystalline GaN nanowires, J. Phys. Chem. B 109 (2005) 11095.
[38] X.F. Duan, C.M. Liber, Laser-assisted catalytic growth of single crystal GaN nanowires, J. Am. Chem. Soc. 122 (2000) 188.
[39] T.Y. Kim, S.H. Lee, Y.H. Mo, H.W. Shim, K.S. Nahm, E.-K. Suh, J.W. Yang, K.Y. Lim, G.S. Park, Growth of GaN nanowires on Si substrate using Ni catalyst in vertical chemical vapor deposition reactor, J. Cryst. Growth 257 (2003) 97.
[40] T.Y. Kim, S.H. Lee, Y.H. Mo, H.W. Shim, K.S. Nahm, E.-K. Suh, G.S. Park, Growth of GaN nanowires on Si substrate using Ni catalyst in vertical chemical vapor deposition reactor, Korean J. Chem. Eng. 21 (2004) 257.
[41] Y. Terada, H. Yoshida, T. Urushido, H. Miyake, K. Hiramatsu, Field emission from GaN self-organized nanotips, Jpn. J. Appl. Phys. 2 (41) (2002) L1194.
[42] P.B. Shah, B.M. Nichols, M.D. Derenge, K.A. Jones, Sub-100 nm radius of curvature wide-band gap III-nitride vacuum microelectronic field emitter structures created by inductively coupled plasma etching, J. Vac. Sci. Technol. A 22 (1847) (2004).
[43] C.A. Brau, High-brightness photoelectric field-emission cathodes for free-electron laser applications, Nucl. Instr. Meth. A 393 (1997) 426.
[44] Yu. Pozhela, K. Pozhela, P. Raguotis, V. Juciene, Transport in quantum well of GaAs at high electric field, Semiconductors 43 (2009) 1177–1181.
[45] V.G. Mokerov, I.S. Vasilesky, B. Galiev, Yu Pozhela, Drift velocity of electrons in the quantum well at high electric fields, Semiconductors 43 (2009) 458–462.
[46] A. Evtukh, H. Hartnagel, V. Litovchenko, O. Yulmazoglu, Two mechanism of negative dynamic conductivity and generation of oscillations in field-emission structures, Mater. Sci. Eng. A 353 (2003) 27–35.
[47] B. Danilchenko, Determination of the LO phonons lifetime in GaN, Ukr. J. Phys. 54 (2009) 137–142.
[48] V. Litovchenko, A. Evtukh, Vacu um nanoelectronics, in handbook of semiconductor nanostructures and nanodevices, in: A.A. Balandin, K.L. Wang (Eds.), Spintronics and Nanoelectronics, Vol. 3, American Scientific Publishers, Los Angeles, 2006, pp. 153–234.
[49] V. Litovchenko, A.A. Grigoryev, Determination of the electron affinity (work function) of semiconductor nanocrystals, Ukr. J. Phys. 52 (897) (2007).
[50] A.A. Evtukh, V.G. Litovchenko, N.I. Klyui, M.O. Semenenko, E.B. Kaganovich, E.G. Manoilov, Int. J. Nanotechnol. 3 (2006) 283–299.
[51] V. Litovchenko, A. Evtukh, O. Yilmazoglu, K. Mutamba, H.L. Hartnagel, D. Pavlidis, Gunn effect in the field-emission phenomena, J. Appl. Phys. 97 (2005) 044911.
[52] V. Litovchenko, A. Grigoriev, A. Evtukh, O. Yilmazoglu, H. Hartnagel, D. Pavlidis, Electron field emission from wide bandgap semiconductors under intervalley carrier redistribution, J. Appl. Phys. 106 (2009) (104511-1-104511-7).
[53] V.G. Litovchenko, Emission characterisrics of semiconductor quantum cathodes, Ukr. J. Phys. 54 (2009) 181–186.
[54] A. Evtukh, O. Yilmazoglu, V. Litovchenko, M. Semenenko, T. Gorbanyuk, A. Grygoriev, H. Hartnagel, Electron field emission from nanostructured surfaces of GaN and AlGaN, Phys. Stat. Sol. (C) 5 (2008) 425.
[55] U.V. Bhapkar, M.S. Shur, Monte Carlo calculation of velocity-field characteristics of wurtzite GaN, J. Appl. Phys. 82 (1997) 1649.
[56] V. Litovchenko, A. Evtukh, Yu. Kruchenko, N. Goncharuk, O. Yilmazoglu, K. Mutamba, H.L. Hartnagel, D. Pavlidis, Quantum size resonance tunneling in the field emission phenomenon, J. Appl. Phys. 96 (2004) 867.
[57] V.G. Litovchenko, A.A. Evtukh, Yu M. Litvin, N.M. Goncharuk, H. Hartnagel, O. Yilmazoglu, D. Pavlidis, Peculiarities of the electron field emission from quantum-size structures, Appl. Surf. Sci. 215 (2003) 160.
[58] O. Yilmazoglu, D. Pavlidis, Yu M. Litvin, S. Hubbard, I.M. Tiginyanu, K. Mutamba, H.L. Hartnagel, V.G. Litovchenko, A. Evtukh, Field emission from quantum size GaN structures, Appl. Surf. Sci. 220 (2003) 46.
[59] O. Yilmazoglu, D. Pavlidis, H.L. Hartnagel, A. Evtukh, V. Litovchenko, N. Semenenko, Evidence of satellite valley position in GaN by photoexcited field emission spectroscopy, J. Appl. Phys. 103 (2008) 114511.
[60] V. Litovchenko, A. Evtukh, O. Yilmazoglu, K. Mutamba, H.L. Hartnagel, D. Pavlidis, Gunn effect in the field-emission phenomena, J. Appl. Phys. 97 (2005) 044911.
[61] S. Sze, Modern Semiconductor Device Physics, Wiley, New York, 1998.
[62] R.J. Nemanich, Electron affinity of AlN, GaN and AlGaN alloys, in: J.H. Edgar, S. Strite, I. Akasaki, H. Amano, C. Wetzel (Eds.), Properties, Processing and Applications of Gallium Nitride and Related Semiconductors, INSPEC, London, 1999, pp. 98–103.
[63] V. Bugrov, M. Levinstein, S. Rumyantserv, A. Zubrilov, Advanced Semiconductor Materials, Wiley, New York, 2001, pp. 1–30.
[64] N. Morgulis, About field emission composite semiconductor cathodes, J. Tech. Phys. 17 (983) (1947) (in Russian).
[65] R. Stratton, Energy distributions of field emitted electrons, Phys. Rev. 135 (1964) A794.
[66] B. Van Zeghbroeck, Principles of Semiconductor Devices (tutorial), 2007 http://ecee.colorado.edu/~bart/book/book/index.html.
[67] J. Kolnik, I.H. Oguzman, K.F. Brennan, Electronic transport studies of bulk zincblende and wurtzite phases of GaN based on an ensemble Monte Carlo calculation including a full zone band structure, J. Appl. Phys. 78 (1995) 1033.
[68] J.M. Barker, D.K. Ferry, D.D. Koleske, R.J. Shul, Bulk GaN and AlGaN/GaN heterostructure drift velocity measurements and comparison to theoretical models, J. Appl. Phys. 97 (2005) 063705.
[69] V. Dienys, J. Pozela, Hot Electrons, Mintis, Vilnius, 1971.
[70] V.I. Gavrilenko, A.M. Grekhov, D.V. Korbutjak, V.G. Litovchenko, Optical Properties of Semiconductors, Naukova Dumka, Kiev, 1987.
[71] Yu. Pozela, K. Pozela, V. Juciene, S. Balakauskas, V.P. Evtikhiev, A.S. Schkolnik, Yu. Storasta, A. Mekys, An increase in the electron mobility in the two-barrier AlGaAs/GaAs/AlGaAs heterostructure as a result of introduction of thin InAs barriers for polar optical phonons into the GaAs quantum well, Semiconductors 41 (2007) 1439.
[72] V.G. Mokerov, Yu. K. Pozela, Yu.V. Fedorov, Electron transport in unipolar heterostructure transistors with quantum dots in strong electric fields, Semiconductors 37 (2003) 1217.
[73] J. Pozela, K. Pozela, V. Juciene, Electron mobility and electron scattering by polar optical phonons in heterostructure quantum wells, Semiconductors 34 (2000) 1011.
[74] C. Youtsey, L.T. Romano, R.J. Molnar, I. Adesida, Rapid evaluation of dislocation densities in n-type GaN films using photoenhanced wet etching, Appl. Phys. Lett. 74 (3537) (1999).
[75] T. Utsumi, Vacuum microelectronics. What's new and exciting, IEEE Trans. Electron. Dev. 38 (2276) (1991).
[76] M.S. Shur, M.A. Khan, GaN and Related Materials II, in: S.J. Pearton (Ed.), Gordon and Breach, New York, 1999.
[77] S. Nakamura, GaN and Related Materials II, in: S.J. Pearton (Ed.), Gordon and Breach, New York, 1999.
[78] Y.C. Yeo, T.C. Chong, M.F. Li, Electronic band structures and effective-mass parameters of wurtzite GaN and InN, J. Appl. Phys. 83 (1429) 1998.
[79] C. Bulutay, B.K. Ridley, N.A. Zakhleniuk, Full-band polar optical phonon scattering analysis and negative differential conductivity in wurtzite GaN, Phys. Rev. B 62 (2000) 15754.
[80] C.-K. Sun, Y.-L. Huang, S. Keller, U.K. Mishra, S.P. DenBaars, Ultrafast electron dynamics study of GaN, Phys. Rev. B 59 (1999) 13535.
[81] M.E. Levinshtein, S.L. Rumyantsev, M.S. Shur, Properties of Advanced Semiconductor Materials: GaN, AlN, InN, BN, SiC, SiGe, Wiley, New York, 2001.
[82] Z. Liu, F. Machuca, P. Pianetta, W.E. Spider, R.F.W. Pease, Electron scattering study within the depletion region of the GaN(0001) and the GaAs(100) surface, Appl. Phys. Lett. 85 (1541) 2004.
[83] M. Cardona, K.L. Shaklee, F.H. Pollak, Electroreflectance at a semiconductor-electrolyte interface, Phys. Rev. 154 (1967) 696.
[84] E. Kisker, K. Shroder, M. Campagna, W. Gudat, Temperature dependence of the exchange splitting of Fe by spin-resolved photoemission spectroscopy with synchrotron radiation, Phys. Rev. Lett. 52 (1984) 2285.

[85] R.D. Young, Theoretical total-energy distribution of field-emitted electrons, Phys. Rev. 113 (1959) 110.
[86] R.D. Young, H.E. Clark, Effect of surface patch fields on field-emission work-function determinations, Phys. Rev. Lett. 17 (1966) 351.
[87] R.D. Young, E.W. Muller, Progress in field-emission work-function measurements of atomically perfect crystal planes, J. Appl. Phys. 33 (1962) 91.
[88] T. Radon, Photofield emission spectroscopy, Prog. Surf. Sci. 59 (1998) 331.
[89] B.I. Lundqvist, K. Mountfield, J.W. Wilkins, Photo-field-emission: a new probe of electron states between the Fermi and vacuum levels, Solid State Commun. 10 (1972) 383.
[90] M.J.G. Lee, R. Reifenberger, Periodic field-dependent photocurrent from a tungsten field emitter, Surf. Sci. 70 (1978) 114.
[91] A. Evtukh, O. Yilmazoglu, V. Litovchenko, M. Semenenko, O. Kyriienko, H.L. Hartnagel, D. Pavlidis, Peculiarities of the photon-assisted field emissions from GaN nanorods, J. Vac. Sci. Technol. B 28 (2010) C2A72.